EJN fens EUROPEAN JOURNAL OF NEUROSCIENCE

European Journal of Neuroscience, Vol. 30, pp. 2077–2088, 2009 doi:10.1111/j.1460-9568.2009.06997.x

SYNAPTIC MECHANISMS

Short-term synaptic plasticity at the main and vomeronasal olfactory receptor to mitral cell synapse in frog

K. R. Delaney,[1] E. Y. Qnais[2,*] and A. B. Hardy[1,†]
[1]Department of Biology, University of Victoria, Victoria, BC V8W 3N5, Canada
[2]Biological Sciences, Simon Fraser University, Burnaby, BC, Canada

Keywords: accessory olfactory bulb, GABAB, paired-pulse facilitation, presynaptic inbition, pre-terminal calcuim

Abstract

Synaptic responses resulting from stimulation of the main olfactory and vomeronasal (VN) nerves were measured in main and accessory olfactory bulb (AOB) of frog, *Rana pipiens*, to test the hypothesis that properties of these synapses would reflect the distinct differences in the time course of odour delivery to each of these olfactory structures. Paired-pulse depression dominated responses to repetitive stimulation of the main olfactory nerve for interstimulus intervals (ISI) up to several seconds. Inhibition of voltage-gated Ca^{2+} channels by GABAB receptors contributes significantly to this inhibition of transmitter release, particularly for ISI > 0.5 s. In contrast, the monosynaptic connection between VN sensory neurons and mitral cells in the AOB showed enhancement with pairs or short trains of stimuli for ISI of 0.5 to > 10 s. A small inhibitory effect of GABAB receptors on presynaptic Ca^{2+} influx and release was only evident when a large proportion of the VN axons were stimulated simultaneously but even with inhibition present an overall enhancement of release was observed. Increasing the number of conditioning stimuli from one to five increased residual [Ca^{2+}] and enhancement but a direct correlation between residual [Ca^{2+}] and either the magnitude or the time course of enhancement was not observed. Enhanced transmitter release from VN afferent terminals results in effective integration of sustained low-frequency activity, which may play a role in the detection of low-intensity odourant stimuli by the VN system.

Introduction

Olfactory stimuli are received, processed and relayed to higher brain centres by separate main and accessory olfactory systems. In frogs the vomeronasal (VN) organ projects to a physically distinct accessory olfactory bulb (AOB) visible as a hemispherical lobe on the ventrolateral surface of the caudal portion of the main olfactory bulb (MOB). Mitral cells (MCs) of the MOB project primarily to lateral aspects of the telencephalon while projections from the AOB are directed exclusively to the amygdala (Scalia *et al.*, 1991; Mulligan *et al.*, 2001) and in turn to the hypothalamus. The major cell types of the MOB, mitral, granule and periglomerular, are found in the AOB but a distinct difference of the MCs in AOB of mammals, as well as lower groups, is the projection of apical dendrites to multiple glomeruli. The MOB receives extensive centrifugal input from several caudal brain regions while the AOB receives direct synaptic input only from the sensory afferents of the VN organ (Scalia *et al.*, 1991). This simpler AOB circuitry along with the ease of maintaining the olfactory neural and epithelial tissue of frogs *in vitro* facilitates physiological analysis of synaptic functions of the olfactory system (Delaney & Hall, 1996). Here we focus on the temporal properties of the first input synapse in the MOB and AOB from the sensory afferents to the MCs. Information on the nature of the stimuli that activate the VN organ in frogs is lacking but it is likely that they produce sustained activation of VN receptors as seen in rodents (Liman & Corey, 1996; Keverne, 1999) given that the frog VN organ is similarly located in a pocket within the medial sinus cavity with a restricted opening that inhibits rapid flow-through of odourant molecules (Nowack & Wöhrmann-Repenning, 2009). The odour transduction mechanisms of VN and olfactory sensory neurons differ substantially, and mammalian VN receptors respond to sustained current injection with sustained firing and little adaptation, in contrast to olfactory sensory neurons, which require pulsatile current injection to maintain firing (Liman & Corey, 1996; Takami, 2002). Given the differences in types of odours and the time course of exposure of the receptors, we hypothesized that differences would be seen in the temporal properties of the synapses transferring odour signals from the VN organ to AOB as compared with the main olfactory epithelium to the MOB.

Repetitive synaptic activity changes synaptic strength by altering transmitter release properties at virtually all synapses. These changes in synaptic strength can either increase or decrease transmission and can persist for a few seconds or as long as several days. Activity-dependent changes in synaptic strength expand the computational repertoire of neural circuits as they can be used to implement various mathematical transforms that are equivalent to high-pass filtering, feedback inhibition or temporal integration, within a single element (the presynaptic terminal) rather than through the interconnection of many elements in a specifically designed circuit (Natschlager *et al.*, 2001).

Correspondence: Dr K. R. Delaney, as above.
E-mail: kdelaney@uvic.ca

**Present address*: Department of Biology, Hashemite University, Zarqa, Jordon.

†*Present address*: Department of Physiology, University of Toronto, Toronto, ON M5S 1A8, Canada.

Received 27 October 2008, revised 10 August 2009, accepted 20 September 2009

Originally characterized most extensively at vertebrate neuromuscular junctions, presynaptic, short-term, activity-dependent synaptic enhancement (ADE) has been found to be remarkably consistent across synapses of vertebrate and invertebrate species with respect to the time course of recovery after stimulation and the effects of increasing the number and frequency of stimuli in the conditioning train (Zucker & Regehr, 2002). Enhanced transmission that decays within a few seconds following one or a few action potentials is traditionally called facilitation or paired-pulse facilitation (Magleby, 1987). At many synapses, stimulating tens or hundreds of action potentials induces additional release-enhancing processes that reverse more slowly after the cessation of stimulation such as augmentation (5–10 s) or post-tetanic potentiation lasting tens of seconds to many minutes. Although the temporal properties of these different phases of presynaptic ADE are relatively consistent between different synapses and species, there is considerable difference in the extent that different phases are emphasized or absent at any particular synapse.

The ubiquity of ADE within nervous systems combined with the variety with which different phases (e.g. paired-pulse facilitation vs. augmentation) are emphasized at different synapses suggests that ADE can be tuned to adapt the frequency-dependent properties of information transfer at different synapses to the specific challenges each synapse faces. Here we report on ADE at VN sensory neuron to AOB MC synapses in frog brain that is distinctive with respect to its magnitude and persistence relative to the amount of presynaptic activity required to induce it. ADE at this synapse operates over a frequency range from approximately 0.1 to 3 Hz, can potentially double the strength of transmission 1–2 s after a single VN sensory neuron action potential and is maximized by firing 5–10 action potentials. Combined with a lack of adaptation by some VN sensory neurons, low-frequency ADE at VN–MC synapses would be expected to enhance the detection of low concentrations of odourants that are persistent in the environment.

Materials and methods

All experimental procedures were carried out in accordance with Canadian Animal Care Council Regulations and approved by Simon Fraser University and University of Victoria Animal Care and Use committees. All efforts were made to minimize the number of animals used.

Tissue preparation

Adult male frogs (*Rana pipiens*), 2.5–3.5 inches in length, were used (Charles D. Sullivan Co., Nashville, TN, USA). The animals were acclimated to room temperature (21–24°C) for at least 7 days before experiments and fed live crickets or worms. Frogs were decapitated after anaesthesia by immersion in buffered 200 μM MS222 and the head immediately submerged in chilled artificial cerebral spinal fluid (ACSF) solution (in mM: 120 NaCl, 2 KCl, 26 $NaHCO_3$, 2.5 NaH_2PO_4, 0.5 Na_2HPO_4, 10 D-glucose, 1.5 $MgCl_2$ and 2 $CaCl_2$ bubbled with carbogen, 95%/5% O_2/CO_2, pH 7.4–7.5). The bone of the ventral cranium was removed in a caudal to rostral direction using fine rongeurs up to the point where the main olfactory and VN nerve pass through the bone en route to the olfactory sensory epithelium. The olfactory nerves were cut and the forebrain including the anterior half of the telencephalon and MOB/AOB was removed from the brain case. The AOB consists of a spherical protrusion from the ventrolateral surface of the posterior portion of the MOB. The VN nerve, which forms a tract of axons on the surface of the olfactory nerve (ON) was separated from the ON to allow electrical stimulation of the VN sensory neuron axons. In most of the experiments, the forebrain was hemisected longitudinally by cutting through the interbulbar adhesion. One forebrain hemisphere was used immediately while the other was kept in a separate chilled bath of carbogenated ACSF solution at 5°C for later use. The preparation was secured to the bottom of a 2-ml Sylgard^{TM}-lined recording chamber, lateral side up, with 0.1-mm minuten pins through the main ON and the edges of the telencephalon. The preparation was perfused with carbogenated ACSF at a rate of 1–3 mL/min. All experiments were performed at room temperature (21–24°C) to which the frogs had been previously acclimated.

Stimulation and recording parameters

Synaptic responses were elicited by applying square wave current pulses of 200-μs duration and 0.08–3 mA using a stimulus isolation unit (SIU90, Cygnus Technology, Delaware Water Gap, PA) controlled by a digital stimulator (model PG4000; Cygnus Technology or Master-8 A.M.PI, Jerusalem, Israel), through a plastic suction electrode (outer diameter 300–500 μm) into which the VN axons had been sucked. To test paired-pulse enhancement, pairs of stimuli were applied with interstimulus intervals (ISIs) of 0.1–65 s. The interval between pairs of stimuli was always 2 min. Enhancement was quantified by dividing the peak amplitude of the second response by the amplitude of the first response, with the result expressed as a percentage. To test enhancement induced by a train of action potentials, we applied a conditioning train of five stimuli at 2 Hz, followed by a test pulse at intervals of 0.5–60 s after the end of the train. This was done with 2–3 min between conditioning trains.

Changes in synaptic strength induced by trains of action potentials were quantified by dividing the amplitude of the post-stimulus test response by the amplitude of the first response in the train, with the result expressed as a percentage. In both paired-pulse and train-induced enhancement, the decay rate was characterized by fitting exponential functions to the decay phase. To stimulate MCs antidromically, a bipolar, enamel-coated stainless steel or silver electrode was placed on fibres of the accessory olfactory tract (AOT) that emerge from the AOB and project along the ventricular surface of the medial wall of the telencephalon to the amygdala (Scalia *et al.*, 1991; Mulligan *et al.*, 2001). The electrode was placed 1–3 mm from the AOB and square wave pulses of 200-μs duration were applied. Threshold responses were obtained at about 0.1 mA, maximal responses at around 0.3 mA.

Whole-cell recordings

Whole-cell recordings were obtained in both voltage and current clamp configurations. Patch electrodes were pulled from borosilicate capillary glass (1.16 mm i.d., 1.5 mm o.d., PG 150T-10; Warner Instrument Corp., Hamden, CT, USA) with a resistance of 8–10 MΩ when filled with internal solution. This range provided a balance between minimizing damage during passes through the tissue and having sufficient electrical and diffusional access to the intracellular space after breakthrough. Voltage clamp experiments were terminated if access resistance exceeded 20 MΩ. In some experiments the electrodes were coated with melted dental periphery wax (Surgident^{TM}, Heraeus Kulzer, USA) or wrapped with Parafilm^{TM} to reduce capacitive current. Positive pressure was applied to the pipette while it was advanced and monitored using an in-line digital pressure meter. A long-working-distance oblique illumination condenser (Olympus) allowed for visually assisted patching of neurons in some cases. Many recordings were obtained by 'blind' patching using the following

procedure. Positive pressure of 0.5 p.s.i. was applied as electrodes were advanced into the AOB while repeatedly applying voltage steps (1 mV, 10 ms). Once the electrode entered the tissue the positive pressure was reduced to 0.15 p.s.i., and the electrode was advanced rapidly 100–200 μm below the brain surface. The electrode was then advanced in 1–2-μm steps. When the electrode resistance increased, suggesting contact with a cell, the positive pressure was removed and slight negative pressure (approximately 0–0.3 p.s.i.) was applied. After obtaining a GΩ seal a holding potential of −60 to −65 mV was applied and breakthrough was achieved by applying brief pulses of negative pressure. Patch clamp recordings (Model 501A, Warner Instruments Corp.) were filtered at 2 kHz with a four-pole Bessel filter, digitized at 5–10 kHz with an Instrunet^{TM} A/D converter (model 100B; GW Instruments Inc., Somerville, MA, USA), acquired using SUPERSCOPE II software and analysed off-line with commercial software (IGOR PRO^{TM}, Wavemetrics, Portland, OR, USA).

For current clamp recordings electrodes were filled with a K^+ methanesulfonate-based solution (in mM: 75 K-methanesulfonate, 10 HEPES, 1 EGTA, 1 $CaCl_2$, 4 $MgCl_2$, 3ATP-Na, 0.3 GTP-Na, biocytin 0.2–0.5%, pH 7.3). For voltage clamp recordings, electrodes were filled with a Cs-methanesulfonate-based intracellular solution (in mM: 55 Cs-methanesulfonate, 15 TEA-Cl, 10 HEPES, 10 QX314-Cl, 10 EGTA, 1 $CaCl_2$, 3 $MgCl_2$, 2ATP-Na, 0.3 GTP-Na, biocytin 0.2–0.5%, pH 7.3–7.4). In some experiments 10 mM EGTA was replaced by 10 mM BAPTA. The access resistance was monitored periodically and experiments were rejected if this parameter exceeded 50 MΩ during recording. For current clamp experiments, cells with a resting membrane potential more negative than −50 mV were accepted for analysis. All current clamp data have been corrected for a +7-mV junction potential. MCs were identified based on their distance from the surface (200–400 μm), the presence of spontaneous inhibitory postsynaptic currents, lack of spontaneous excitatory postsynaptic currents, their input impedance and an AOT-stimulation-evoked, antidromic spike. In addition, in about half of the experiments, the electrode contained biocytin (0.2–0.5%) and the cell type was confirmed anatomically following recording.

Field potential recordings

To record local field potentials resulting from VN nerve stimulation ACSF-filled glass microelectrodes with a 3–5-μm tip diameter were placed on the surface or into the glomerular layer approximately 50 μm below the dorsal surface, in the caudal half of the AOB hemisphere where VN afferents synapse onto distal MC dendrites. VN nerve compound action potentials (volleys) were measured using an ACSF-filled glass electrode placed on the surface of the VN nerve 100–200 μm before it entered the AOB. Presynaptic fibre volleys were monitored throughout the experiments to ensure that no major changes in fibre excitability occurred, and also that they differed by less than 10% between the first stimulus in the conditioning train (either a train of five stimuli at 2 Hz or single stimulus) and a test stimulus 1 s after the conditioning pulse.

Anatomical characterization of the VN nerve

In order to confirm that axons from all parts of the VN are distributed to all or most glomeruli, the VN nerve was split and each half of the nerve sucked into a pipette containing either dextran-conjugated Rhodamine Green (10 000 mol. wt) or Texas Red 10 000 (10 000 mol. wt) (Invitrogen Inc., Burlington, ON, Canada). Nerve terminals were filled by a 6–12-h application of the dyes while the tissue was held in cold oxygen saturated saline (5°C)

Cell identification

Biocytin-filled neurons were reacted for horseradish peroxidase histochemistry according to previously published procedures with some modifications (Tago *et al.*, 1986). Briefly, the brains were fixed after electrophysiological recording for at least 24 h in cold (4°C) 4% paraformaldehyde in phosphate-buffered saline (PBS, 0.1 M), pH 7.3. The brains were embedded in agar (5%), sectioned (300 μm) on a vibrating microtome (Pelco Vibratome 1000, Ted Pella, Inc, CA, USA), collected in PBS and incubated for 20 min in 1% hydrogen peroxidase. The sections were then rinsed several times with phosphate buffer (0.1 M). Injected cells were labelled by incubating the sections with an avidin–horseradish peroxidase complex (standard ABC kit, Vector Labs, Burlingame, CA, USA) at a dilution of 1 : 250 in a 1% solution of Triton X-100 prepared with PBS for 24–48 h. After several rinses in Tris-buffered saline (0.05 M) over 1 h, the sections were reacted with diaminobenzidine (0.025%), H_2O_2 (0.03%) and imidazole (5%) in 0.05 M Tris buffer for 10–20 min. The sections were rinsed and mounted on gelatin-coated slides, air-dried, dehydrated through a graded alcohol series and coverslipped in Permount^{TM}. Images of stained neurons were acquired under bright-field illumination. For data on the morphology of labelled neurons, some cells were reconstructed using a 100× oil-immersion objective lens, from serial sections (usually not more than two) using a custom set-up consisting of a microscope interfaced via stage encoders and a drawing tube directed towards the monitor of a Macintosh computer running IGOR PRO^{TM} software. Images of other stained neurons were acquired under bright-field illumination and then reconstructed by tracing over images in Adobe Photoshop.

Fluorometric detection of Ca^{2+} transients

VN terminals were filled with the Ca^{2+}-sensitive dye Fluo-4 dextran conjugate (10 000 mol. wt, K_D ~4 μM), applied to the cut stump of the VN that was drawn into a plastic pipette. The tissue was maintained in a large bath of carbogenated ACSF for 6–10 h at 5°C for loading. A 40× lens (Olympus 0.8 NA, water-immersion) was used to image the filled terminals and a field stop diaphragm was used to restrict excitation light to a 150-μm-diameter region in the middle of the AOB where the nerve terminals were well filled. Excitation light from a T.I.L.L. Polychrome II^{TM} switching monochrometer (485 nm centre wavelength) was attenuated by 75%, then passed through a 485 ± 15-nm bandpass filter, reflected by a dichroic beam splitter (DCLP 505), and emitted fluorescence was collected through a 530 ± 20-nm emission filter (Chroma Corp., Brattleboro, VT, USA). Fluorescence was detected with a photomultiplier tube (Hamamatsu, H5783-04, Japan). Fluorescence responses were corrected for tissue fluorescence then normalized as fractional changes according to

$$\Delta F/F = (F_{(t)} - F_0)/F_0 - B$$

where F_0 = total fluorescence over 1s prior to stimulation of the VN, $F_{(t)}$ = total fluorescence at times after stimulation of the VN, and B = tissue autofluorescence measured from an adjacent region of MOB at the end of the experiment.

We estimated that [Ca^{2+}] changes on the order of 100–200 nM were produced by single action potentials using the fractional saturation method of Feller *et al.* (1996) after loading terminals with the high-affinity indicator Ca^{2+} Green-1 dextran (data not shown). Changes of this magnitude produce changes in fluorescence of the low-affinity indicator Fluo-4 dextran that are essentially linearly proportional to ΔF (Mulligan *et al.*, 2001) so no further calibration of the indicator was performed and only values of $\Delta F/F$ are reported.

EGTA loading

To increase endogenous buffer capacity in the terminals, EGTA was loaded by bath application of EGTA-AM. Aliquots of 100 mM EGTA-AM in dimethyl sulfoxide (DMSO) were prepared and frozen at −20°C. Aliquots were diluted immediately before use in ACSF to final EGTA concentrations of 20 μM and 0.1% DMSO and sonicated for 2–3 min and applied to the tissue for 30–45 min. During EGTA loading, perfusion with ACSF was stopped and the oxygen and pH levels were maintained by directly bubbling pre-moisturized carbogen through the fluid in the chamber. The gas mixture was delivered via a ring of plastic tubing embedded in the Sylgard™ lining the bottom around the periphery of the main chamber of the dish. Pinholes (15–20) in the wall of the plastic tube created a sprinkler-type bubbling, which was controlled by a manual valve. The physiological stability of preparations in the static bath was carefully examined in several control experiments and the evoked synaptic and Ca^{2+} responses were found to be stable over the course of several hours. To confirm there was no effect of DMSO on ADE, basal synaptic transmission or Ca^{2+} influx control experiments were performed with application of ACSF containing 0.1% DMSO.

Drugs

Chemicals for intracellular and extracellular solutions were obtained from Sigma except QX314 (Alomone Labs, Jerusalem, Israel). The following drugs (Precision Biochemicals Inc, Canada) were used: bicuculline methiodide, a GABAA receptor antagonist; D-2-amino-5 phosphovalerate (APV), an NMDA receptor antagonist; 6,7-dinitro-quinoxaline-2,3-dione, (DNQX), an AMPA receptor antagonist; 1S, 3R-1-aminocyclopentane-1,3-dicarboxylic acid, (ACPD), a group I and II metabotropic glutamate receptor (mGluR) agonist; quisqualate, a broad-spectrum agonist of mGluR and non-NMDA receptors; and CGP 55845 or CGP 35348, GABAB receptor (GABAB-R) antagonists (a gift from Novartis Canada Inc.). Drugs were applied by superfusion in ACSF for at least 15–50 min to establish equilibrium in the tissue.

Data analysis

Results are expressed as mean ± SE unless otherwise stated. Data from different drug-treated conditions were compared using a paired or unpaired Student's *t*-test as appropriate. Statistical significance was defined at $P < 0.05$.

Results

Neurotransmission between sensory neurons and mitral cells of the main and accessory bulbs

Figure 1 shows the distinct difference between the response of main and accessory olfactory bulb (MOB, AOB) circuits to repetitive electrical stimulation of the primary afferent axons in the olfactory and vomeronasal (ON, VN) nerves, respectively. A pronounced decrease in the local field potential (LFP) response to repeated stimuli is seen in the MOB with a corresponding decline in the amplitude of the postsynaptic potentials measured in MCs. These responses are similar to previously published data for rat, mouse and turtle MOB (Eng & Kocsis, 1987; Keller *et al.*, 1998; Mutoh *et al.*, 2005). The characteristic paired pulse depression (PPD) response of the ON-evoked synaptic response in the MOB is maximal at an ISI of about 0.5 s and reverses over the course of 10–20 s (Fig. 2). PPD is associated with a decrease in action potential-mediated Ca^{2+} influx, which is maximal at

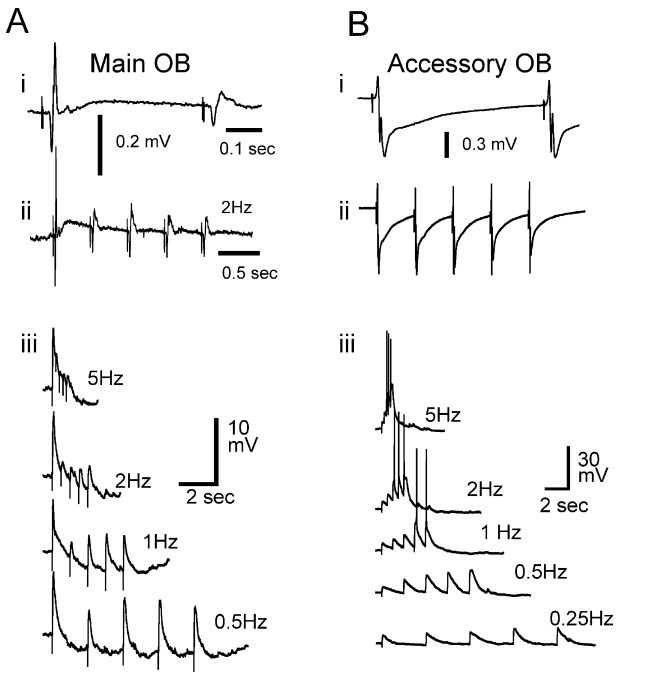

FIG. 1. Post synaptic potentials (PSPs) in a mitral cell evoked by trains of stimuli applied to main olfactory (A) and vomeronasal (B) nerves at different frequencies. Traces i and ii show local field potential responses in the MOB or AOB to a pair and a short train of olfactory or VN nerve stimuli. Inhibition dominates in the MOB (A) so that repetitive stimulation is not effective for bringing MCs to threshold. In AOB mitral cells the PSP lasts > 1 s and with repetitive stimulation shows pronounced enhancement, even at low (e.g. 0.5 Hz) frequencies. Consequently at the stimulus intensity used for this example, MCs respond to higher frequencies (e.g. 5, 2 and 1 Hz) with spikes due to a combination of temporal summation and activity-dependent enhancement.

an ISI of 0.5 s and also proportionately greater as more ON afferents are recruited (Fig. 2C). This is reflected as an increase in PPD as stimulus intensity is increased to recruit more afferent axons. The ON in adult *R. pipiens* extends 1–2 mm anterior to the OB, allowing it to be surgically divided into two bundles, each of which can be stimulated separately (Fig. 3). Stimulating one set of axons depresses the response to stimulation evoked by another inactive set of axons when these are subsequently activated with a delay of a few hundred milliseconds or more. This stimulus paradigm eliminates neurotransmitter depletion from the primary afferent as a dominant factor in PPD of the MOB. Both self- and crossed-fibre inhibition are accompanied by a reduction of action potential-mediated presynaptic Ca^{2+} influx (Figs 2C and 3E). The GABAB-R antagonist CGP55485 antagonizes both self- and cross-fibre PPD (Fig. 3B–D) and reverses the inhibition of action potential-evoked presynaptic Ca^{2+} influx in ON terminals (Fig. 3B, E and F). Inhibition of transmission at intervals greater than 1 s was blocked by CGP55485 with little effect for intervals less than 0.5 s (Fig. 3, Fii).

In the contrast to the robust activity-dependent depression at the main ON to MC synapse, the VN afferent to MC synapse in the AOB shows remarkable low-frequency ADE, which is evident in the local field potential as well as intracellular recordings from MCs (Figs 1B and 6A).

To study the neurotransmission between VN sensory and MCs synapses in intact AOB, local field potential and whole-cell recordings from MCs were obtained. A combination of blind and visually directed whole-cell patching was used and cell type was confirmed by correlating electrophysiological characteristics with morphology as revealed by biocytin staining.

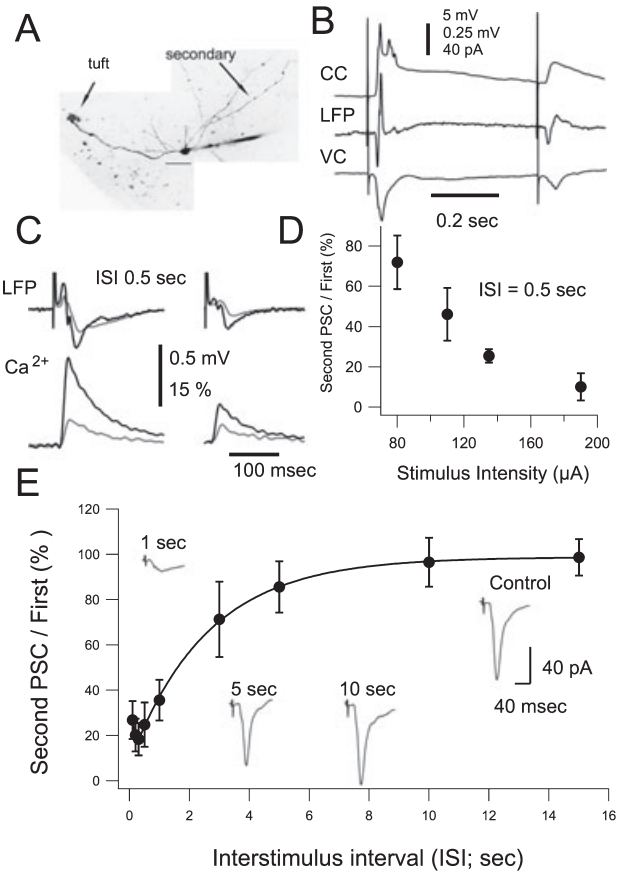

FIG. 2. In the MOB, the ON to MC synapse shows paired pulse depression (PPD). (A) Two-photon fluorescence reconstruction of an MC filled with Alexa-fluor 488. The dark thick line on the right is the recording pipette. (B) Current clamp (CC) local field potential (LFP) and voltage clamp recordings showing a decrease in the response to the second or a pair of ON stimuli delivered at an interstimulus interval (ISI) of 0.5 s. (C) PPD increases with increasing ON stimulus intensity. Black traces are responses to 80 μA stimulation, grey traces 200 μA. PPD is expressed as the ratio of the second to the first postsynaptic current evoked by a pair of ON stimuli. (D) PPD as a function of ISI (n = 3). PPD is maximal at about 0.5 s and decays within about 10 s. (E) Time course of recovery from PPD after a strong (200 μA) stimulus. Scale bar in A is 50 μm.

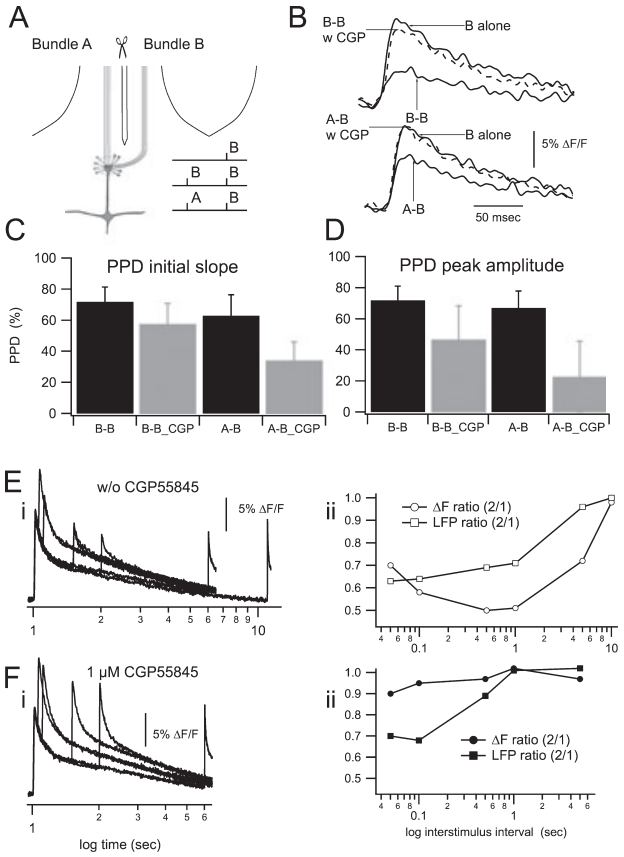

FIG. 3. PPD in the MOB crosses from stimulated to unstimulated terminals. (A) ON split into to halves, A and B, each of which is independently stimulated as shown. (B) Top traces: stimulating bundle B inhibits Ca^{2+} influx at synapses activated by stimulating bundle B again (B-B), which is relieved by 10 μM CGP55845. Lower traces: stimulating bundle A also inhibits Ca^{2+} influx into terminals activated 0.5 s later by stimulating bundle B (A-B). This inhibition is also relieved by CGP55485. Scale bars: 10 pA and 20 ms. (C) 10 μM CGP55845 relieves approximately half the PPD of the postsynaptic current (PSC) measured by whole-cell recording from an MC, assessed by measuring the maximum slope of the initial inward PSC 10–14 ms after onset, or (D) the peak amplitude of the complex PSC. 10–20 postsynaptic responses for each cell and each treatment were averaged and the bars are means ± SD of the average PPD for nine different cells. (E) panel i, Fluo-4 dextran fluorescence transients elicited by pairs of ON stimuli at various intervals showing inhibition of Ca^{2+} influx in the absence of GABAB receptor block. Panel ii, ratios of second to first Ca^{2+} transient amplitudes (circles) and local field potential (squares) recorded simultaneously in response to pairs of stimuli at each inter-stimulus interval. (F) Same as (E) after blockade of GABAB receptors. Log time scales in panels Ei and Fi indicate relative time on a logarithmic scale such that 1 corresponds to the time of first stimulus at 0 seconds, 2 corresponds to an inter-stimulus interval of 1 second and so on.

In the AOB, MCs are readily distinguished from granule cells (GCs) (Fig. 4). GCs have diffusely branching dendrites that project from the interior of the spherical AOB superficially and laterally, extending up to and even into the glomerular layer. The GC dendrites display large spines that give them a typical thorny appearance (Fig. 4C). MCs are characterized by smooth, apically orientated dendrites that project up to 300–400 μm from the soma, typically branching several times before producing small tufts in the glomerular layer. Their anatomy is strikingly similar to MCs of the rat AOB (Takami & Graziadei, 1991). Although usually tufts were located at the end of dendrites we also observed what appeared to be tufts in the middle of dendrites in some cells, as illustrated in Fig. 4B. Axons bearing numerous *en passant* synaptic boutons emanated laterally and internally from the somata or proximal primary dendrites (e.g. Fig. 4B). Unlike MCs of the MOB, long laterally orientated secondary dendrites were not seen in AOB MCs. This suggests that as in mammalian AOB the dendrodendritic synapses between MCs and GCs in the AOB are located on the apical dendrites (Takami & Graziadei, 1991), in contrast to their predominant location on secondary (lateral) dendrites in the MOB. MCs could be distinguished from GCs on the basis of their electrophysiological properties, which are similar to their counterparts in the MOB. Input impedance was lower for MCs (375 ± 105 MΩ, n = 4) than for GCs (770 ± 180 MΩ, n = 4). Spontaneous excitatory synaptic currents were observed more infrequently in MCs (< 1/s) than in GCs (> 5/s). Antidromic activation of the AOB, via stimulation of the AOT, evoked an action potential current in 70% of MCs. In addition, a delayed barrage of unitary bicuculline (BIC)-sensitive synaptic currents that reversed around −30 mV was seen in all MCs following AOT stimulation. An inward synaptic current preceded either (antidromic) action potentials or BIC-sensitive synaptic currents. On the other hand, all GCs responded to AOT stimulation with a delayed BIC-insensitive inward synaptic current that reversed at depolarized potentials near 0 mV.

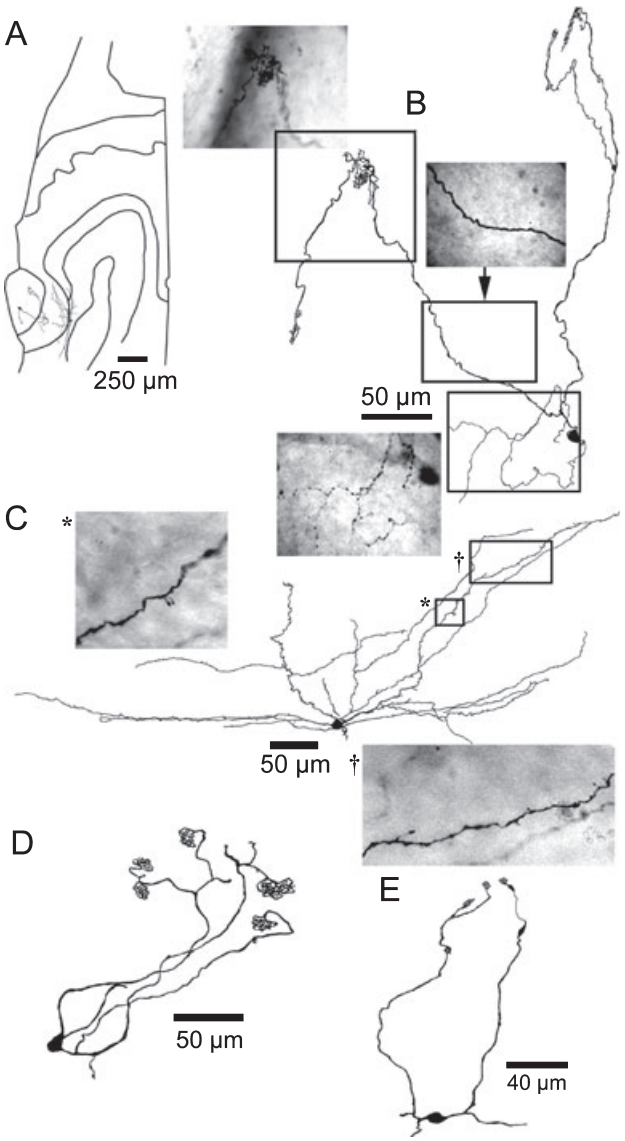

FIG. 4. Morphology of a mitral (MC) and a granule cell (GC) in frog accessory olfactory bulb (AOB). (A) Schematic drawing of a horizontal section through the main and accessory OB showing the position of the cells presented in B and C. (B) Reconstruction of biocytin-filled MC from horizontal AOB sections (300 μm). Insets: photomicrographs from regions indicted by boxes showing a glomerular tuft, smooth dendrites terminating in glomeruli, and a beaded axon that arises from the cell body. (C) GC reconstructed from 300-μm horizontal sections of AOB. Insets: photomicrographs of the regions delineated by the boxes as indicated by * and †. Note that the GC has widely branching dendrites that have a low density of often long necked spines. (D, E) Reconstructions of two more MCs showing several terminal tufts in different glomeruli.

Synaptic responses to VN inputs have not previously been investigated in the frog AOB. We confirmed that excitatory responses evoked by VN stimulation were mediated by glutamatergic receptors as they are in mammals (Jia *et al.*, 1999). A single electrical stimulus of the VN nerve produced a compound inward current upon which smaller, late unitary BIC-sensitive currents were superimposed. These unitary currents were reversed by holding potentials positive to the calculated Cl^- reversal (Fig. 5B), consistent with activation of GABAA receptors. Application of 10–20 μM BIC had only a small effect on the amplitude of early VN–MC-evoked postsynaptic current (PSC), but increased the half-decay time (the time for PSC to decay to 50% of the peak) by 400 ± 30% (n = 4) compared with responses recorded in normal ACSF (Fig. 5A). Bath-applied DNQX (10 μM) plus DL-AP5 (100 μM) greatly reduced, but did not completely block, the VN-evoked PSC (Fig. 5C and D). To test the relative contribution of AMPA-kainate vs. NMDA-dependent components of PSC we sequentially added DNQX and AP5 in the presence of 10 μM BIC while holding at −60 mV. AP5 (100 μM, n = 4) caused a decrease in the amplitude of 12 ± 3% (n = 4) and a decrease in the half-decay time of 50 ± 10% (n = 4) compared with responses recorded in the presence of 10–20 μM BIC alone (Fig. 5C). Co-application of 10 μM DNQX, 100 μM AP5 and BIC left a small inward current with a delayed time to peak and a slow decay (Fig. 5C). This indicates that the majority of the excitatory PSC at −60 mV holding potential is mediated by AMPA/kainate receptors. Increasing DNQX concentration to 100 μM blocked the remaining current (Fig. 2F, data representative of three experiments). VN-evoked responses recovered to 60–80% of pre-block levels 30–60 min after washout of AP5 and DNQX (71 ± 12%, n = 3). As little NMDA-R-mediated current was seen at −60 mV (Fig. 5D), cells were held at −25 mV to uncover the NMDA-R component. At this holding potential BIC (10–20 μM) now blocked a delayed outward current (presumably disynaptic) to reveal a long-lasting (300–500 ms) inward current, most of which was blocked by AP5 (Fig. 5E).

It is potentially problematic to achieve reliable voltage clamp of VN nerve-evoked synaptic currents as MCs have long apical dendrites and VN synapses occur at the distal tuft. Apical dendrites are fortunately relatively large in diameter and unbranched over most of their length. Estimates of the reversal potential for AMPA-R- and NMDA-R-mediated synaptic currents obtained by voltage clamp were within +5 to +10 mV of theoretical predictions for the stimulus intensities that were used to calculate ADE, suggesting voltage errors and unclamped active currents were not significantly biasing our estimates of postsynaptic current amplitudes (Fig. 5G and H).

Paired-pulse enhancement of the VN nerve synaptic response is seen in the AOB–LFP and whole-cell recordings from MCs in both voltage and current clamp modes (Fig. 6A). Unlike ON–MOB synapses the VN–AOB paired pulse plasticity does not depend strongly on the number of VN afferents that are stimulated (Fig. 6B). Paired pulse enhancement is maximal at an ISI of about 1–2 s (Fig. 6C) and recovers approximately exponentially over the course of 30–60 s (fitted line, tau = 12 s). Little or no change is seen in the amplitude of the afferent volley measured from the surface of the VN nerve (inset box; Fig. 6C) or the input impedance, suggesting that paired-pulse enhancement is not due to increased VN axon excitability. Most forms of ADE are sensitive to the frequency and number of conditioning stimuli. We stimulated the VN nerve five times at 2 Hz and measured the enhancement of the VN afferent to MC synapse at intervals after the end of the train. Figure 6D shows that enhancement was slightly greater with this paradigm than with a single conditioning stimulus and recovered with a similar exponential time course, although a little more slowly (fitted line, tau = 15.7 s).

In order to identify the locus of this enhanced synaptic connection from VN afferents to MCs, we performed experiments to probe possible presynaptic and postsynaptic mechanisms. To determine whether the enhancement was restricted to activated synapses or could cross over to other synapses, we split the VN nerve in half and stimulated each bundle of axons independently. Stimulating each bundle independently showed that MCs received input from both sets of axons, and we confirmed the projection of both sets of axons to the same glomeruli by filling one bundle with Rhodamine Green dextran and the other with Texas Red dextran (Fig. 7). Although enhancement was seen with repetitive stimulation of either bundle, no evidence

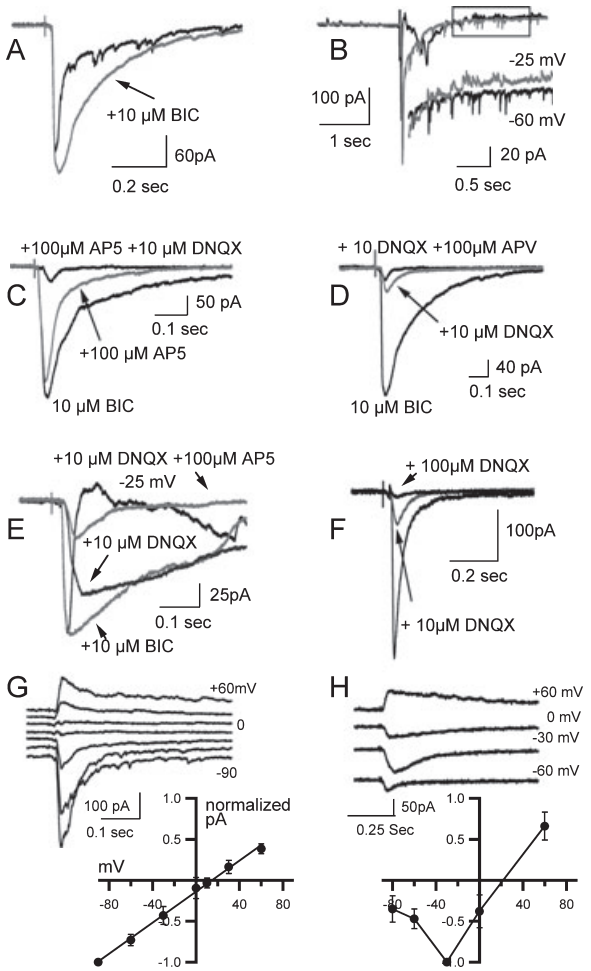

FIG. 5. Excitatory and inhibitory synaptic potentials in voltage-clamped MCs. Cells were held at −60 mV except for E where the cell was held at −25 mV (grey traces) while stimulating the VN nerve electrically to generate synaptic currents. (A) Application of bicuculline (BIC; 10–20 μM) suppressed the unitary synaptic currents and slowed the decay of MC response. (B) The delayed onset unitary currents reversed when the membrane potential was held above the calculated reversal potential for Cl^-, consistent with synaptic events mediated by GABAA receptors. Lower pair of traces shows a higher resolution view of the section of the upper traces enclosed by the box. Scale bars refer to upper pair of traces. (C) Application of AP5 (100 μM) in the presence of BIC caused a small decrease in the amplitude and shortened the inward current. Further addition of 10 μM DNQX blocked all but a small inward current with delayed activation and intermediate decay rate. (D and E). Response mediated by NMDA receptors is isolated by co-application of DNQX (10 μM) and BIC at a holding potential of −60 mV where it is small (D) and increased by holding at −25 mV (E). The inward current that is insensitive to BIC+DNQX is significantly suppressed by addition of 100 μM AP5. (F) Holding at −60 mV the small inward current that remained in the presence of 10 μM DNQX, AP5 and BIC was blocked by increasing DNQX to 100 μM. (G and H) Current vs. voltage relationships and reversal potentials for pharmacologically isolated AMPA-kainate and NMDA-dependent synaptic currents (n = 3).

was obtained for the transfer of enhancement from stimulated to un-stimulated synapses following a conditioning train of five stimuli at 2 Hz. Thus, unlike the pronounced activity-dependent depression of olfactory receptor cell to MC synapses in the MOB, the dominant form of activity-dependent plasticity at VN to MC synapses in AOB is restricted to active synapses.

Glutamate released by VN afferents activates both AMPA-kainate and NMDA-type receptors on MCs. Using a combination of voltage and pharmacological blockers we observed that NMDA-R and AMPA-kainate receptor-dependent postsynaptic currents were equally enhanced by paired-pulse and train stimuli (Fig. 8). Activation of mGluR receptors with 50 μM ACPD had no observable effect on the amplitude of excitatory postsynaptic currents (EPSCs) or the time course of ADE (n = 3). Using 100 μM DNQX and a holding potential of +40 mV to isolate the NMDA-R-dependent component we saw no effect of 25–50 μM quisqualate on EPSC amplitude or ADE time course (n = 3 experiments). Also, inclusion of 10 mM BAPTA in the recording pipette had no effect on the magnitude or time course of ADE, suggesting postsynaptic Ca^{2+} elevation is not needed for enhancement. Twenty minutes after breakthrough, enhancement 1 s after a five-stimulus 2-Hz conditioning train was 260 ± 17% (n = 4) for BAPTA-containing cells compared with 245 ± 7% (n = 3) for non-BAPTA cells. ADE recovery time course was 16 ± 2.3 s (n = 4) and 17 ± 2 s (n = 3) for BAPTA and non-BAPTA cells, respectively. The results of experiments presented thus far point to a presynaptic locus for the expression of ADE at VN–MC synapses in AOB.

The duration and amplitude of ADE enhancement at the VN nerve to MC synapse are both striking considering the small number and low frequency of conditioning stimuli that produce it. With regard to the small number of conditioning stimuli needed, this resembles short-term facilitation, also commonly termed paired-pulse facilitation, seen at other synapses including neuromuscular junctions. With respect to the time course of decay, it is similar to synaptic augmentation or weakly activated post-tetanic potentiation (Magleby, 1987; Zucker & Regehr, 2002). In a variety of synapses these forms of enhancement depend on presynaptic Ca^{2+} elevation. Augmentation and post-tetanic potentiation are well correlated with residual Ca^{2+} in the bulk of the cytoplasm in many synapses (Delaney & Tank, 1994; Zucker & Regehr, 2002) whereas paired-pulse facilitation is sensitive to the kinetics of Ca^{2+} elevation within a few milliseconds of its entry into the terminal. We therefore undertook to manipulate presynaptic Ca^{2+} levels during conditioning stimuli in order to determine whether ADE was dependent on this factor.

VN terminals were anterogradely filled with a low-affinity dextran-conjugated Ca^{2+} indicator (Fluo-4 dextran; KD ∼4 μM, Invitrogen) through the cut axons of the VN nerve to measure the increase and recovery of [Ca^{2+}] in presynaptic terminals. To confirm that addition of Fluo-4 dextran had minimal effects on ADE, test pulses were delivered after a train of five conditioning stimuli in preparations filled (n = 3) and not filled (n = 4) with indicator. One second after the conditioning train the enhancement of the PSC was 246 ± 15% (n = 3) with Fluo-4 and 260 ± 7% (n = 4) without Fluo-4. Exponential fitting to the data also revealed no change in the ADE decay rate (tau = 15.5 ± 2.2 s for filled, n = 3; 17.1 ± 1.3 s, n = 4 for unfilled). Despite the small size of presynaptic terminals the removal rate for Ca^{2+} is slow, requiring 10–15 s to recover completely after even a single action potential. While increasing the number of times the VN axons were stimulated from one to five had only a minor effect on the amplitude and rate of decay of ADE (see Fig. 6), Ca^{2+} accumulation was strongly dependent on the number of stimuli (Fig. 9A and B) and with each succeeding stimulus the transient increase in fluorescence was similar to that preceding it, provided stimulus intensity was maintained less than or equal to 3–4 times threshold. This stimulus intensity range was used for all experiments except those to investigate GABAB-R-mediated inhibition which used high-intensity stimulation as described later in this report (see Fig. 9E). Likewise, there was no significant increase in the Ca^{2+} influx to a single action potential tested at various times after one (small residual Ca^{2+}) or five (greater residual Ca^{2+}) action potentials (Fig. 9A). One, 3 and 7 s after a single stimulus the ΔF transient was 104 ± 1.2, 103 ± 0.5 and 1.5 ± 0.5% of the initial stimulus transient (n = 3 preparations). One, 3 and 7 s after

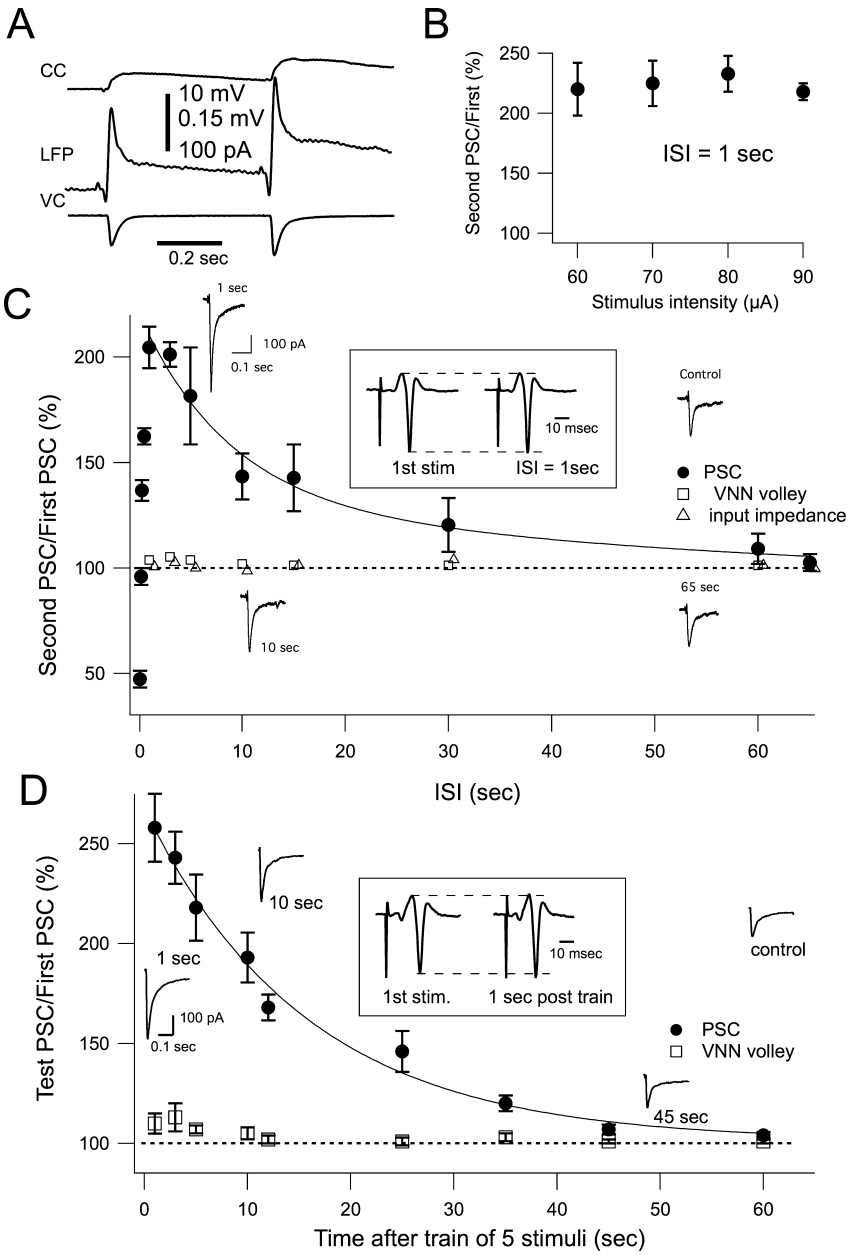

FIG. 6. Activity-dependent enhancement of VN to MC synapses in AOB. (A) The EPSP (top), local field potential (middle) and EPSC (bottom) exhibit paired-pulse enhancement over a wide range of nerve stimulus intensities (B). (C) Paired pulse enhancement plotted against ISIs (each solid circle is the mean ± SE for five averaged stimuli from five different cells). The data are overlaid with a single exponential with a time constant of 11.3 s (solid line, fit begins at 1 s ISI). The individual data sets, each fitted with an exponential, resulted in a time constant of decay of 12.6 ± 3.7 s (n = 5). Sample responses from a paired-pulse enhancement experiment are shown around averaged data. Open boxes are averaged VN nerve field potentials. Triangles are input impedance measurements. Error bars for VN nerve and impedance measurements are the same size as the data points and not presented to avoid obscuring the data. Impedance data points are offset by 0.5 s to avoid overlap with VN data points. Boxed inset: example field potentials recorded from the VN nerve. (D) Decay of enhancement of test EPSCs following a train of five conditioning stimuli delivered at 2 Hz (circles, n = 5). Open boxes are data for the normalized VN nerve afferent volley amplitude.

the last of five stimuli delivered at 0.5 Hz the ΔF transient was 109 ± 2.0, 107 ± 3.2 and 104 ± 2.1% of the ΔF transient of the first stimulus in the train (n = 3). This is consistent with a constant influx of Ca^{2+} per action potential given the low Ca^{2+} affinity of the indicator for which dye saturation is not a factor, and the lack of evidence for an increase in the number of stimulated axons following repeated stimulation (see Fig. 6C and D inset).

Although enhancement increased with five vs. one conditioning stimulus, the amount of enhanced transmission after a train is primarily a function of the time after a train rather than the $[Ca^{2+}]$ (Fig. 9B and C). After stimulation, the Ca^{2+} requires many seconds to recover, which considering the small size of the terminals is unexpectedly slow, but the time course of ADE is consistently slower (Fig. 9C) and the magnitude of ADE does not correlate well with the magnitude of change in cytoplasmic $[Ca^{2+}]$ at any time after stimulation. For example, 10 s after a single stimulus $[Ca^{2+}]$ has nearly recovered to pre-stimulus levels while transmission is still increased by as much as 50% over basal levels (Fig. 9B and C).

Paired-pulse facilitation has been shown to be sensitive to buffers such as EGTA that have slow to moderate forward binding rates

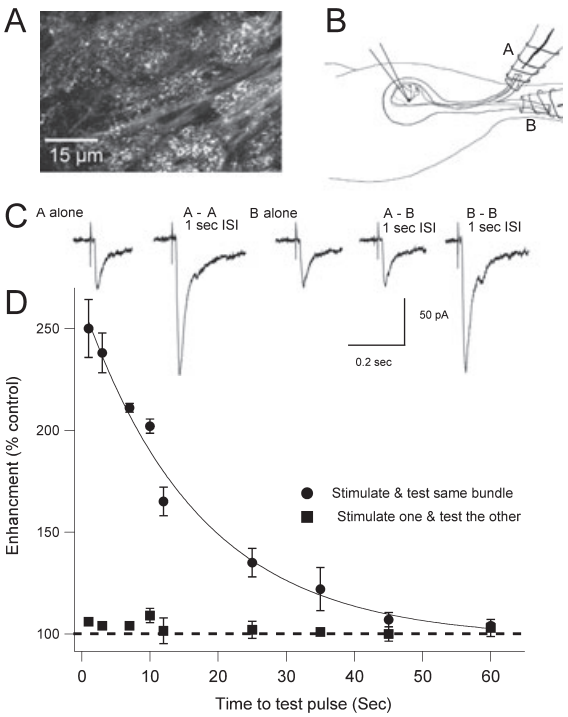

FIG. 7. Activity-dependent enhancement does not cross from stimulated to unstimulated terminals. (A) The VN nerve was surgically split and VN sensory nerve terminals were anterogradely filled with Texas Red dextran to confirm that the projection of terminals from half the nerve to all glomeruli in the AOB. (C) Example EPSCs resulting from activation of one bundle followed by itself 1 s later (A-A; B-B) or one bundle then the other (A–B). (D) After a train of five conditioning stimuli delivered at a rate of 2 Hz to bundle A the resulting test EPSCs evoked by a single bundle A stimulus (same bundle; filled circles) are enhanced while bundle B responses (other; filled squares) are unaffected.

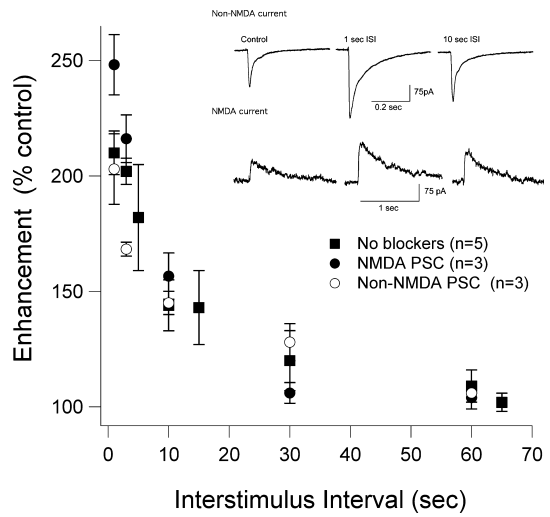

FIG. 8. NMDA-R- and non-NMDA-R-dependent EPSCs are equally enhanced following repetitive stimulation, suggesting a change in postsynaptic receptor number or sensitivity is not occurring.

(Feller *et al.*, 1996) as these can compete effectively for Ca^{2+} acting at facilitating sites while having minimal effects on transmission itself. We bath-applied an acetyl methyl ester form of EGTA (EGTA-AM) to increase the buffer capacity of presynaptic terminals. To confirm that buffer capacity had been increased we compared the recovery rate of elevated cytoplasmic $[Ca^{2+}]$ back to resting levels following stimulation of presynaptic action potentials, before and after incubation with EGTA-AM (Fig. 9D). EGTA caused a slight attenuation of the individual peak fluorescence transients (< 5%), pronounced acceleration of the initial recovery phase and a slower than normal late-stage recovery of $[Ca^{2+}]$. These changes are all consistent with an increase in Ca^{2+} buffer capacity by addition of a slow forward rate buffer (Feller *et al.*, 1996). The first LFP was unaffected by EGTA (< 10% difference between pre EGTA and post EGTA across three experiments), which is expected given that the slow forward rate of the buffer does not allow it to compete effectively with the transmitter release mechanism (Adler *et al.*, 1991). EGTA reduced the sum of the transient peak and the residual of the fluorescence by 44 ± 4.9% as tested in three preparations at three intervals (0.5, 1 and 2 s), after a single stimulus (pair-wise Student's *t*-test, $P < 0.005$; $n = 9$). Despite clear effects on the residual $[Ca^{2+}]$ following a conditioning stimulus there was no measurable effect on the ADE of the LFP measured at the same times (Fig. 9, Dii, right).

Finally, by way of comparison with the prominent GABAB-R-mediated PPD of Ca^{2+} influx seen at ON to MC synapses in the MOB we used measurements of Fluo-4 dextran fluorescence in VN afferent terminals to explore whether there was evidence for GABAB-R activity there. As shown in Fig. 9E, there was an attenuation of the fluorescence transients during repetitive stimulation only when the stimulus intensity was increased to saturating levels, approximately 1 mA, which is 5–10 times the threshold stimulus intensity and corresponds to levels 2–3 times greater than those used in all other experiments presented. The attenuation was barely detectable for a pair of stimuli but increased during a five-stimulus train. Bath application of CGP55485 restored the fluorescence transient during the train to approximately 90% of its initial value ($n = 3$). These data indicate that GABAB-R activation can reduce presynaptic Ca^{2+} currents at VN afferent terminals but it is only recruited by stimuli that synchronously activate the majority of afferents.

Paired pulse type facilitation is usually unchanged or increased when release probability is reduced by lowering extracellular $[Ca^{2+}]$ (Magleby, 1987), whereas synaptic augmentation and post-tetantic potentiation that depend on sustained, small to moderate increases in cytoplasmic $[Ca^{2+}]$ following tetanic stimulation are typically reduced. Lowering extracellular $[Ca^{2+}]$ from 2 to 0.5 mM decreases the action potential-mediated Ca^{2+} influx as well as the buildup of cytoplasmic $[Ca^{2+}]$ in VN terminals during trains (Fig. 10). Low extracellular $[Ca^{2+}]$ did not reduce the magnitude or the time course of ADE between 1 and 50 s following a conditioning train of five stimuli at 2 Hz. Up to a five-fold buildup of enhancement is seen during a 0.5-Hz train in 0.4 mM extracellular $[Ca^{2+}]$ (Fig. 10B). In addition, ADE tested 3 and 10 s following a single stimulus is, if anything, increased by lowering extracellular $[Ca^{2+}]$ from 2 to 0.4 mM (Fig. 10C).

Discussion

In this study we compare the low-frequency, activity-dependent properties of the olfactory sensory afferent to MC synapse in the frog MOB and AOB. In both systems the odour-evoked responses of the sensory neuron are reinforced by the properties of their synapses with their respective MCs. Olfactory receptors of the main olfactory epithelium respond to sustained odour application and depolarizing current injection with transient action potential firing (Liman & Corey, 1996; Reisert & Matthews, 1999). The response of the primary afferent synapse in the MOB to repetitive presynaptic activity is dominated by depression rather than enhancement over a wide range

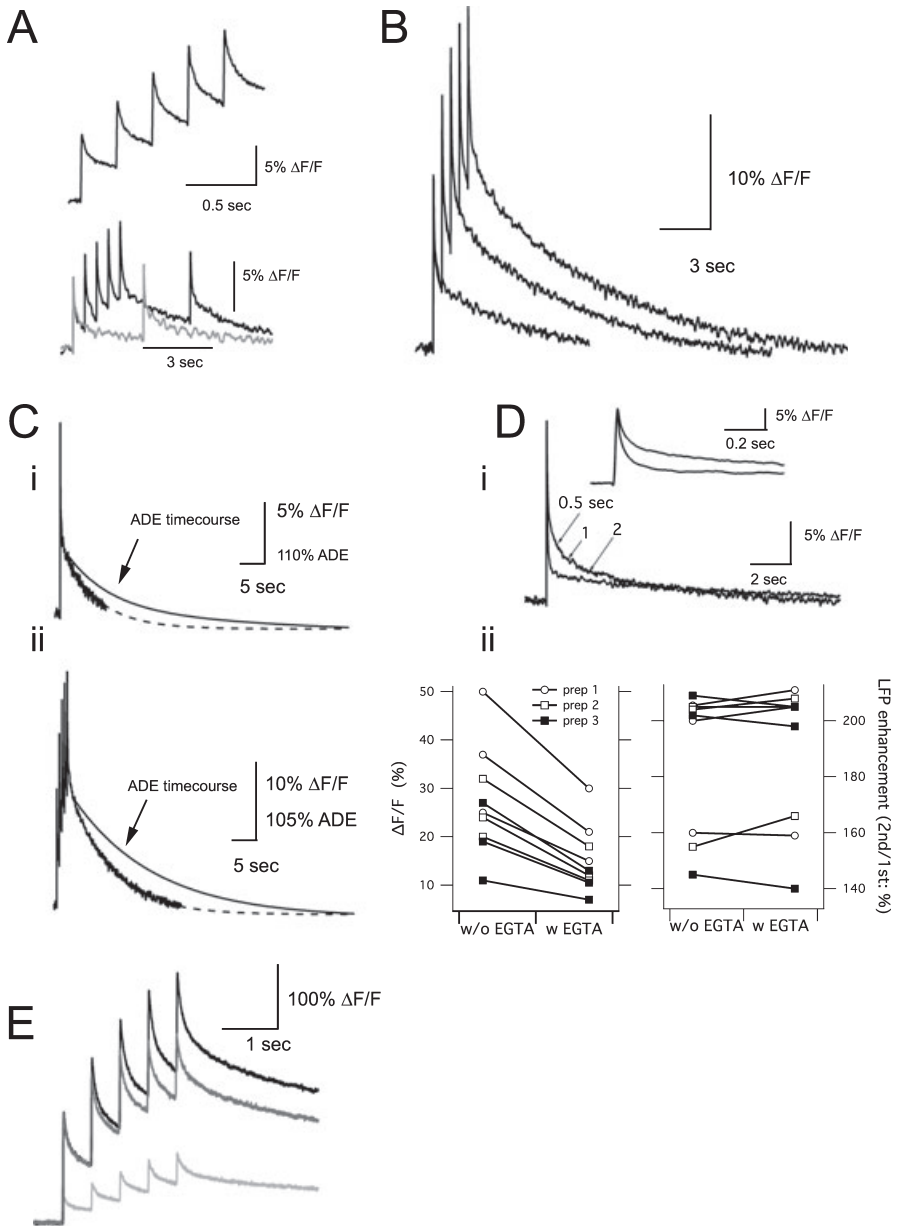

FIG. 9. [Ca^{2+}] build up and recovery in VN terminals during and after repetitive stimulation. (A) At low to moderate stimulus intensities Ca^{2+} influx per action potential remains constant and residual [Ca^{2+}] accumulates to higher levels with more action potentials. After conditioning stimulation the Ca^{2+} influx per action potential does not increase. (B) The same residual [Ca^{2+}] is present at later times after trains of three compared with two or one action potential (e.g. dashed line) due to greater buildup with more action potentials. In the example shown residual [Ca^{2+}] is the same at 6, 13 and 17 s after the last stimulus while enhancement is 185, 157 or 151%, respectively. (C) Time course of recovery of residual [Ca^{2+}] (dashed line) compared with synaptic enhancement after a single stimulus (i) or a train of five stimuli (ii). The dashed lines are fitted exponentials for the Ca^{2+} measurements, which are extrapolated to later times for comparison with the time course of synaptic enhancement. The synaptic enhancement is shown as solid lines, which are the exponential fits to the summary data shown in Fig. 6. As one way to try to compare Ca^{2+} with enhancement the data are presented using a scaling in which the amplitudes of the Ca^{2+} and enhancement are matched at 1 and 50 s after the stimulus. (D) (i) Effect of increasing buffer capacity with EGTA-AM application on the recovery of [Ca^{2+}]. (ii) Effect of EGTA loading on residual [Ca^{2+}] and enhancement for three preparations, each one evaluated 0.5, 1 and 2 s after a single conditioning stimulus. (E) Ca^{2+} influx per action potential declines during a train of high-intensity nerve stimuli compared with low intensity (grey traces). This inhibition is blocked by 10 μM CGP55485 (black trace).

of stimulus conditions. Transmission is inhibited for periods of 0.5–15 s by a mechanism that appears to be dominated by GABAB-R-mediated down-regulation of the presynaptic Ca^{2+} current, which increases as more afferents are activated. The increasing inhibition that occurs with increased afferent recruitment tends to normalize the amplitude of the second and subsequent responses in a train of stimuli across a range of intensities and is probably involved in extending the dynamic range of responses of MCs to increasing concentrations of odourants. For shorter ISI other processes such as GABAA-mediated feedback inhibition or vesicle depletion are dominant, the latter being consistent with an intrinsically high release probability for these synapses as reported for rodents (Murphy *et al.*, 2004).

The VN receptor to MC synapse AOB shows little evidence for depression and instead demonstrates a robust ADE in response to low levels of repetitive activation. We performed a series of experiments each of which was consistent with a presynaptic locus for the increased strength of the synapse. Neither increased afferent axon excitability nor increased presynaptic Ca^{2+} channel activity can

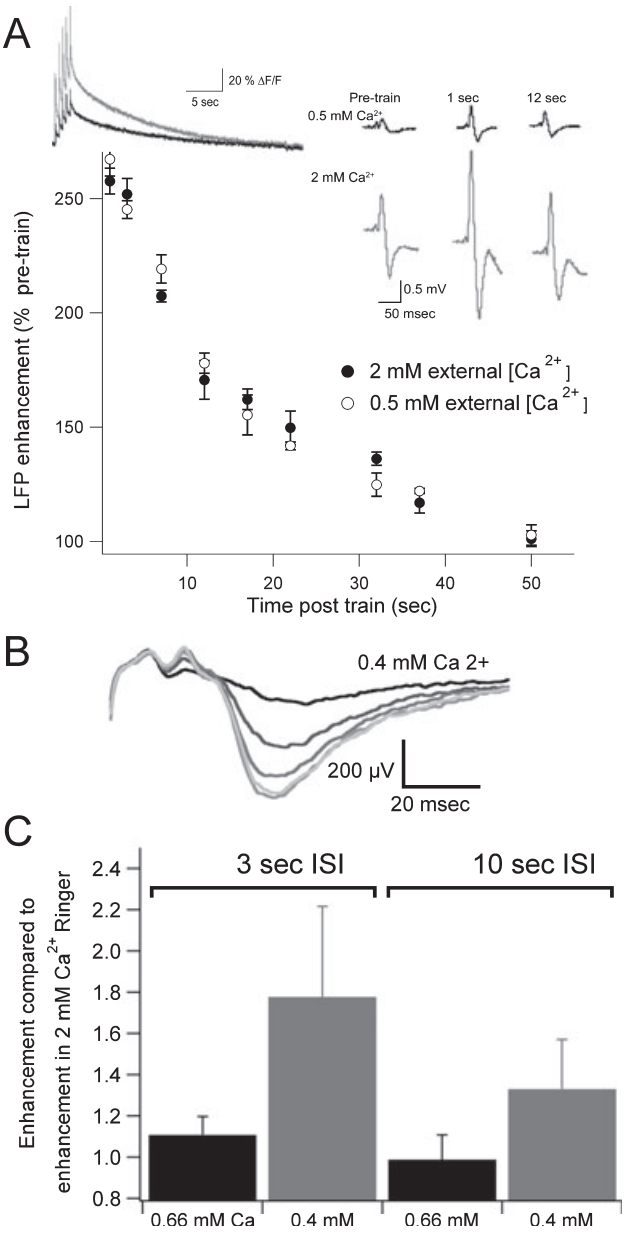

FIG. 10. Lowering extracellular [Ca^{2+}] decreases the action potential-mediated Ca^{2+} current as well as the buildup of cytoplasmic [Ca^{2+}] during trains but does not reduce the enhancement after a train or single stimuli. (A) Upper left inset: Ca^{2+} buildup and recovery during and after a 5-Hz train. Enhancement measured by a single test pulse following a 5-Hz train in normal 2 mM and reduced, 0.5 mM Ca^{2+}-containing Ringer solution. Upper right inset: example LFPs recorded 50 μm below the bulb surface. (B) Buildup of surface recorded LFP enhancement during five successive VN stimuli at an ISI of 2 s in 0.4 mM Ca^{2+}. Black trace, LFP to first stimulus in train progressing to light grey for the fifth response in the train. Data shown are averages of four responses from a single preparation. (C) Enhancement recorded 3 and 10 s after a single VN stimulation in Ringer solution containing 0.66 or 0.4 mM Ca^{2+} (Mg^{2+} replaces Ca^{2+}) compared with enhancement at the same intervals in normal 2 mM Ringer. 1.0 = same amount of enhancement, means ± SEM, n = 3 experiments for 0.4 mM and n = 4 for 0.66 mM.

account for the increased transmitter release at these synapses. The enhancement persists for many seconds after one or a few stimuli delivered at frequencies below 5 Hz. The fact that only a few action potentials are needed to produce enhancement suggests it reflects a short-term or paired-pulse type of facilitation. Although facilitation usually reverses ten times more rapidly than the ADE at VN–MC synapses the phenomenon could nonetheless be a slowly reversing form of facilitation. A characteristic of facilitation is a dependence on the elevation of [Ca^{2+}] in the vicinity of release sites for a few milliseconds after an action potential and as such it is sensitive to slow forward rate buffers, which compete for free Ca^{2+} on this time-scale. However, we were unable to attenuate the enhancement with acetylmethyl ester loading of EGTA, a technique that works well at retinotectal synapses in the same species (Feller *et al.*, 1996). Despite observing an acceleration of the early phase of Ca^{2+} recovery after an action potential with EGTA loading, we cannot rule out the possibility that the levels of increased intracellular Ca^{2+} buffering we were able to achieve were insufficient to effectively compete with facilitatory sites. Another possibility that we cannot discount is that although our imaging confirmed that EGTA loading altered Ca^{2+} handling in a way that should have interfered with classical paired pulse facilitation, these changes and our imaging were limited to superficial terminals while the LFP includes currents generated by superficial and deep terminals.

The time course of the ADE is similar to synaptic augmentation, which normally requires stimulation of many tens of action potentials at neuromuscular junctions and other synapses for its induction. Augmentation is generally attributed to persistently elevated cytoplasmic [Ca^{2+}] (residual Ca^{2+}) (Delaney & Tank, 1994; Zucker & Regehr, 2002). Increasing the number of conditioning stimuli increases the magnitude and time course of enhanced transmission slightly at VN–MC synapses but the enhancement and residual [Ca^{2+}] are not well correlated after a conditioning stimulus of 1–5 action potentials. Although recovery of [Ca^{2+}] after action potentials is slow, requiring many seconds to reach pre-stimulus levels, the decay of the synaptic enhancement is always significantly slower. In this respect as well as the fact that the small number of action potentials and low rate of firing are sufficient to induce ADE, it is strikingly similar to plasticity at the mossy fibre to CA3 synapses in rat hippocampus (Regehr *et al.*, 1994). At mossy synapses residual Ca^{2+} is considered to be responsible for inducing enhanced transmitter release with the reverse rate of the enhancement being much slower than the removal of Ca^{2+} to produce a temporal mismatch such as that observed at VN–MC synapses. However, the lack of effect of reducing extracellular [Ca^{2+}] to as low as 20% of normal (Fig. 10), which reduces the residual cytoplasmic [Ca^{2+}] several seconds after stimulation, argues strongly against an enhancement due to a high-affinity 'augmentation-type' Ca^{2+} mechanism. It also reinforces other experiments that indicate enhancement is not due to release of a neuromodulatory substance as this would also be substantially reduced by low extracellular [Ca^{2+}].

In summary, the small number of stimuli needed to induce enhancement and the marked insensitivity to lowering extracellular [Ca^{2+}] suggests a form of facilitation rather than an augmentation or post-tetanic type of enhancement as a mechanism. The extremely long duration of the enhancement, however, indicates an exceptionally slow reverse rate for the facilitation process compared with that in other central or neuromuscular synapses.

Regardless of the mechanism responsible for the enhanced transmission, it has the effect of increasing coupling between VN receptors and MCs under conditions of repetitive low-frequency activity. Our difficulty in identifying a mechanism for ADE using traditional approaches that manipulate presynaptic [Ca^{2+}] does not alter the fact that ADE exists and VN–AOB signalling is different from that of olfactory afferents to MOB. The magnitude, time course and sensitivity to low-frequency activation of the VN–MC synapse is similar to the mossy fibre to CA3 synapses of rodent hippocampus

(Regehr *et al.*, 1994), which have been suggested to contribute to the integration of the low-frequency burst activity of dentate granule cells observed during exploratory behaviours (Buzsáki & Czeh, 1992; Jung & McNaughton, 1993; Henze *et al.*, 2002). Responses of frog VN receptors to odourants are not known but mammalian VN receptors fire continuously with little or no adaptation during tens of seconds of continuous odour exposure at rates that are proportional to odour concentration. The anatomy of the frog VN organ suggests a fluid pumping mechanism for the delivery of odourant molecules similar to that of mammals (Nowack & Wöhrmann-Repenning, 2009) implying slow sustained exposure of VN afferents to odour signals. Assuming similar properties for amphibian VN receptors, the VN–MC synapse appears well adapted to relaying this sustained activity. We find evidence for some GABAB-R on VN afferent terminals that can reduce Ca^{2+} influx by up to 30% if short trains of high-intensity electrical stimuli that activate the majority of axons are applied to the VN nerve. However, the effect of this inhibition is much weaker than at MOB synapses and unlike the MOB there is little or no cross-fibre modulation of synaptic strength; activity in one set of VN does not alter release at adjacent non-activated synapses, suggesting feedback inhibition that does exist is mainly localized to active synapses.

The properties of VN–MC synapses make them excellent integrators of sustained low-frequency presynaptic activity, which may be relevant to the way in which VN receptors are exposed to odourants and respond to odour stimuli. First, postsynaptic potentials are relatively long-lasting, reflecting the long membrane time constant of the high-impedance MCs so temporal summation is substantial for ISIs up to 500 ms. Second, transmitter depletion is not pronounced and synaptic strength increases up to two-fold following one or a few presynaptic action potentials. The ADE of synaptic strength decays slowly so postsynaptic potentials continue to build in size during repetitive stimulation even with ISIs of several seconds. The low-frequency ADE of the VN–MC synapse could be instrumental in detecting low concentrations of odourants provided these were present for many seconds and would be appropriate for the way in which VN receptors are exposed to odourants within the closed space of the VN organ. It also predicts there should be a pre-exposure effect in which prior exposure to an odourant would enhance subsequent detection, and or discrimination, which could be adaptive in following a discontinuous odour trail. Furthermore, unlike odour receptors of the MOB where cross-adaptation of receptors binding to different odourant molecules is seen, the reduced VN receptor adaptation and the low-frequency ADE of the VN–MC synapse could combine to produce cross-facilitation. For example, a background odourant in the environment would be expected to enhance responses to a second odourant encountered locally if both odourants activate the same VN receptor neuron. Interestingly, as these effects are presynaptic in origin they can develop in the absence of signalling to higher centres. Thus, odourant stimulation too weak to bring an MC to threshold and therefore ineffective to relay information to the amygdala, while not producing an overt behavioural response, could nonetheless modulate the responsiveness of the VN system to continued exposure or exposure to slightly higher concentrations over time scales of several seconds.

Acknowledgement

Work supported by operating grants from the Canadian Institutes for Health Research, MOP 86473 and the Natural Sciences and Engineering Research Council, Canada awarded to KD. EQ received fellowship support from Hashemite University.

Abbreviations

ADE, activity-dependent enhancement; AOB, accessory olfactory bulb; AOT, accessory olfactory tract; EPSC, excitatory postsynaptic current; GC, granule cell; ISI, interstimulus interval; LFP, local field potential; MC, mitral cell; MOB, main olfactory bulb; ON, olfactory nerve; PPD, paired-pulse depression; PSC, post-synaptic current; VN, vomeronasal.

References

Adler, E.M., Augustine, G.J., Duffy, S.N. & Charlton, M.P. (1991) Alien intracellular calcium chelators attenuate neurotransmitter release at the squid giant synapse. *J. Neurosci.*, **11**, 1496–1507.

Buzsáki, G. & Czeh, G. (1992) Physiological function of granule cells: a hypothesis. *Epilepsy Res.*, **7**(Suppl.), 281–290.

Delaney, K.R. & Hall, B.J. (1996) An *in vitro* nose-brain preparation of frog for the study of odor-induced oscillations in olfactory bulb and cortex. *J Neurosci Methods*, **68**, 193–202.

Delaney, K.R. & Tank, D.W. (1994) A quantitative measurement of the dependence of short-term synaptic enhancement on presynaptic residual calcium. *J. Neurosci.*, **14**, 5885–5902.

Eng, D.L. & Kocsis, J.D. (1987) Activity-dependent changes in extracellular potassium and excitability in turtle olfactory nerve. *J. Neurophysiol.*, **57**, 740–754.

Feller, M.B., Delaney, K.R. & Tank, D.W. (1996) Presynaptic calcium dynamics at the frog retinotectal synapse. *J. Neurophysiol.*, **76**, 381–400.

Henze, D.A., Wittner, L. & Buzsáki, G. (2002) Single granule cells reliably discharge targets in the hippocampal CA3 network in vivo. *Nat. Neurosci.*, **5**, 790–795.

Jia, C., Chen, W.R. & Shepherd, G.M. (1999) Synaptic organization and neurotransmitters in the rat accessory olfactory bulb. *J. Neurophysiol.*, **81**, 345–355.

Jung, M.W. & McNaughton, B.L. (1993) Spatial selectivity of unit activity in the hippocampal granular layer. *Hippocampus*, **3**, 165–182.

Keller, A., Yagodin, S., Aroniadou-Anderjaska, V., Zimmer, L.A., Ennis, M., Sheppard, N.F. Jr & Shipley, M.T. (1998) Functional organization of rat olfactory bulb glomeruli revealed by optical imaging. *J. Neurosci.*, **18**, 2602–2612.

Keverne, E.B. (1999) The vomeronasal organ. *Science*, **286**, 716–720.

Liman, E.R. & Corey, D.P. (1996) Electrophysiological characterization of chemosensory neurons from the mouse vomeronasal organ. *J. Neurosci.*, **16**, 4625–4637.

Magleby, K.L. (1987) Short-term changes in synaptic efficacy. In Edelman, G.M., Gall, W.E. & Cowan, W.M. (Eds), *Synaptic Plasticity.* Wiley, New York, pp. 21–56.

Mulligan, S.J., Davison, I. & Delaney, K.R. (2001) Mitral cell presynaptic Ca^{2+} influx and synaptic transmission in frog amygdala. *Neuroscience*, **104**, 137–151.

Murphy, G.J., Glickfeld, L.L., Balsen, Z. & Isaacson, J.S. (2004) Sensory neuron signaling to the brain: properties of the transmitter release from olfactory nerve terminals. *J. Neurosci.*, **24**, 3023–3030.

Mutoh, H., Yuan, Q. & Knöpfel, T. (2005) Long-term depression at olfactory nerve synapses. *J. Neurosci.*, **25**, 4252–4259.

Natschlager, T., Maass, W. & Zador, A. (2001) Efficient temporal processing with biologically realistic dynamic synapses. *Network*, **12**, 75–87.

Nowack, C. & Wöhrmann-Repenning, A. (2009) Anatomical analyses suggest a pumping mechanism for the vomeronasal organ in Anurans. *Copeia*, **1**, 1–6.

Regehr, W.G., Delaney, K.R. & Tank, D.W. (1994) The role of presynaptic calcium in short-term enhancement at the hippocampal mossy fiber synapse. *J. Neurosci.*, **14**, 523–537.

Reisert, J. & Matthews, H.R. (1999) Adaptation of the odour-induced response in frog olfactory receptor cells. *J. Physiol.*, **519**, 801–813.

Scalia, F., Gallousis, G. & Roca, S. (1991) Differential projections of the main and accessory olfactory bulbs in the frog. *J. Comp. Neurol.*, **305**, 443–461.

Tago, H., Kimura, H. & Maeda, T. (1986) Visualization of detailed acetylcholinesterase fiber and neuron staining in rat brain by a sensitive histochemical procedure. *J. Histochem. Cytochem.*, **34**, 1431–1438.

Takami, S. (2002) Recent progress in the neurobiology of the vomeronasal organ. *Microsc. Res. Tech.*, **58**, 228–250.

Takami, S. & Graziadei, P.P. (1991) Light microscopic Golgi study of mitral/tufted cells in the accessory olfactory bulb of the adult rat. *J. Comp. Neurol.*, **311**, 65–83.

Zucker, R.S. & Regehr, W.G. (2002) Short-term synaptic plasticity. *Annu. Rev. Physiol.*, **64**, 355–405.